

# The molecular basis for the inhibition of human cytochrome P450 1A2 by oroxylin and wogonin

Yong-Xian Shao · Peng Zhao · Zhe Li ·  
Ming Liu · Peiqing Liu · Min Huang ·  
Hai-Bin Luo

Received: 18 October 2011 / Revised: 24 November 2011 / Accepted: 6 December 2011 / Published online: 8 January 2012  
© European Biophysical Societies' Association 2012

**Abstract** In our previous kinetics studies the natural products oroxylin and wogonin were shown to have strong biological affinity for, and inhibitory effects against, human cytochrome P450 1A2, with  $IC_{50}$  values of 579 and 248 nM, respectively; this might lead to the occurrence of drug–drug interactions when co-administered clinically. However, their inhibitory mechanisms against 1A2 remain elusive. In this study, molecular docking and molecular dynamics simulations were performed to better understand the molecular basis of their inhibitory mechanisms towards 1A2. Structural analysis revealed that oroxylin has a different binding pattern from wogonin and another very strongly binding inhibitor  $\alpha$ -naphthoflavone (ANF,  $IC_{50} = 49$  nM). The O<sub>7</sub> atom of oroxylin forms hydrogen bonds with the OD1/OD2 atoms of Asp313, which is not observed in the 1A2–wogonin complex. Because of energetically unfavorable repulsions with the methoxy group at the 6 position of the oroxylin ring, significant conformational changes were observed for the sidechain of Thr118 in the MD simulated model. As a result, the larger and much more open binding-site architecture of the 1A2–oroxylin complex may account for its weaker inhibitory

effect relative to the 1A2–ANF complex. Energy analysis indicated that oroxylin has a less negative predicted binding free energy of  $-19.8$  kcal/mol than wogonin ( $-21.1$  kcal/mol), which is consistent with our experimental assays. Additionally, our energy results suggest that van der Waals/hydrophobic and hydrogen-bonding interactions are important in the inhibitory mechanisms of oroxylin whereas the former is the underlying force responsible for strong inhibition by ANF and wogonin.

**Keywords** Oroxylin · Wogonin · CYP 1A2 · Inhibition · Mechanism · Binding free energy

## Introduction

Ubiquitously present in fruits and vegetables, a variety of natural flavonoids have a multitude of pharmacological activity and are therefore of much interest to the pharmaceutical industry and in medicinal chemistry. Several observations reveal that flavonoids can serve as possible chemopreventive agents against environmental mutagens and carcinogens (Birt et al. 2001; Heim et al. 2002; Moon et al. 2006; Ioria et al. 2005; Hong et al. 2004). Flavonoids may be involved in the prevention of malignant transformation by reducing the formation of carcinogens by inhibition of enzymes such as human cytochrome P450 (CYP) 1A1 and 1A2, both of which are known to be involved in carcinogen activation (Heim et al. 2002; Moon et al. 2006; Ioria et al. 2005; Hong et al. 2004). For example,  $\alpha$ -naphthoflavone (ANF) and furafylline are potent inhibitors of 1A2 and help prevent 1A2-mediated chemical carcinogenesis (Cho et al. 2003; Kunze and William 1993). Five human hepatic CYP isoforms (1A2, 2C9, 2C19, 2D6, and 3A4) are known to be involved in CYP-mediated

Yong-Xian Shao and Peng Zhao contributed equally.

**Electronic supplementary material** The online version of this article (doi:10.1007/s00249-011-0785-1) contains supplementary material, which is available to authorized users.

Y.-X. Shao · P. Zhao · Z. Li · M. Liu · P. Liu · M. Huang ·  
H.-B. Luo (✉)  
School of Pharmaceutical Sciences, Sun Yat-Sen University,  
Guangzhou 510006, China  
e-mail: luohb77@mail.sysu.edu.cn

metabolism of approximately 90 % of therapeutic drugs in the human liver (Park et al. 2005; Wolf et al. 2000; Arimoto 2006). Inhibition of human cytochrome P450 has been shown to result in a decrease in P450-mediated metabolism, which sometimes leads to clinically relevant drug–drug interactions (Kemp et al. 2004). 1A2 is one of the major hepatic CYPs expressed in liver tissues, and metabolizes approximately 5–10% of clinical drugs (Faber et al. 2005). It is one of the enzymes responsible for activation of aromatic and heterocyclic amines and polycyclic aromatic hydrocarbons to reactive metabolites (Butler et al. 1989; Eaton et al. 1995).

Oroxylin (5,7-dihydroxy-6-methoxyflavone) is a natural and biologically active flavonoid extracted from the roots of the traditional Chinese herbal medicine Huangqin, *Scutellaria baicalensis* (Li and Chen 2005). It has been widely used for many centuries in traditional oriental medicines for the treatment of various diseases and as a popular antibacterial, antiviral, and anti-inflammatory agent (Li and Chen 2005; Lin and Shieh 1996). Recent research has indicated oroxylin analogues may serve as potential alpha-glucosidase inhibitors (Babu et al. 2008). Wogonin (5,7-dihydroxy-8-methoxyflavone) is another natural flavonoid found in *S. baicalensis*. Wogonin has inhibitory effects on osteolytic bone metastasis of breast cancer (Li-Weber 2009). Additionally, wogonin inhibits diclofenac 4-hydroxylation (CYP 2C9) activity and serves as a competitive inhibitor of CYP 2C9 (Si et al. 2009). In our recent kinetics study (Li et al. 2008), oroxylin and wogonin were shown to have remarkable biological affinity for, and inhibitory effects against, 1A2, with IC<sub>50</sub> values of 579 and 248 nM, respectively, determined by use of an in-vitro “cocktail” method developed by our group (He et al. 2007). However, much less is known about their inhibitory mechanisms against 1A2. It would be of great interest to reveal the molecular basis of the mechanism of inhibition of 1A2 by these two natural products.

Therefore, the objectives of this study were to elucidate the inhibition-binding models of the two natural products, to determine the physicochemical factors affecting their mechanisms of inhibition, and then to use the models to predict their inhibitory potency. To achieve these objectives, molecular docking and molecular dynamics (MD) simulations and MM-PBSA (molecular mechanical and Poisson Boltzmann/surface accessible) binding-free-energy calculations were performed to investigate the molecular basis of binding of the two natural products within the binding-site pocket of 1A2. On the basis of the inhibition-binding models, the key residues within the binding-site pocket which are capable of inducing binding of the two chemicals with 1A2 have been identified. The results of the study can aid the rational molecular design of novel 1A2 inhibitors.

## Experimental methods

### Biological activity

The experimental assays used to investigate the inhibitory potential of ligands against human cytochrome P450 1A2/2C9/2D6/3A4 were based on an in-vitro “cocktail” approach developed in our laboratory as a robust, rapid, and sensitive LC–MS–MS method for determination of the inhibitory affinities of chemicals for CYP enzymes (He et al. 2007). The CYP isoform 1A2 was used in the previous study to obtain inhibitory affinities for 36 flavonoids (Li et al. 2008), and the experimental conditions (including incubation, sample analysis, and calculations) and methods were same as in our recently published article (He et al. 2007). IC<sub>50</sub> values were obtained from triplicate determinations. Among the compounds investigated, oroxylin and wogonin had strong biological activity against 1A2, with IC<sub>50</sub> values of 579 nM (456–702 nM, 95% confidence interval) and 248 nM (177–320 nM, 95% confidence interval), respectively, (Li et al. 2008).

### Molecular docking

The crystal structure of human microsomal P450 1A2 with bound ANF at a resolution 1.95 Å was obtained from the Protein Data Bank (PDB entry: 2HI4) (Sansen et al. 2007), and was used as the initial 3D model. Crystallographic water molecules were deleted from 2HI4, whereas both ANF and the heme group were retained. The N-terminal transmembrane helices were truncated in the crystal structure. To generate the starting models for 1A2 in complexes with oroxylin and wogonin, the molecular modeling program MOE 2008.10 (2008) was used to obtain the docking-binding models. ANF was docked into the active site pocket by use of the automatic docking program, to investigate the conformational space associated with each rotatable bond. The docking parameters in MOE were set as follows: receptor, receptor atoms; binding site, ligands atoms; ligand, ANF (the rotate bonds checkbox was toggled on for the ligands, and bond rotation were performed on the ligand before the placement stage). The placement method, the first scoring function rescoring 1, and the saved poses were alpha triangle, London dG, and 20, respectively. In addition, the refinement, the second refinement scoring function rescoring 2, and the saved poses were set to forcefield, none, and 20, respectively. Poses were generated by superposition of ligand atom triplets and triplets of receptor site points. The receptor site points were alpha sphere centers which represent the locations of tight packing. At each iteration a random conformation was selected, and a random triplet of ligand atoms and a

random triplet of alpha sphere centers were used to determine the pose. Only ligands and amino acid residues within 4.5 Å of the ligands were allowed to move during the minimization. In addition, the remove duplicates checkbox was toggled on to control whether duplicates were to be removed before trimming the pose list. The final refined poses were ranked by MM/GBVI binding free energy estimation (Labute 2008).

Twenty configurations of the ligands were considered in the docking procedures. The root-mean-square deviation (RMSD) values between the docking and initial poses of the ligands were calculated. From the top twenty poses with the highest docking scores, we chose the optimum pose on the basis of both the docking score and cluster popularity. Cluster analysis was carried out on the RMSD values to decide the best docking–binding pose, using an RMSD tolerance of 1.0 Å.

Oroxylin and wogonin were subjected to the same docking procedure. Two systems were then prepared neglecting the 1A2–ANF complex. System 1, named 1A2–oroxylin complex, is 1A2 in complex with oroxylin, whereas system 2, named 1A2–wogonin complex, is 1A2 in complex with wogonin.

#### MD simulations

The docking-initial models for the two systems were prepared using the Xleap module in Amber 10.0 (Case et al. 2008). The antechamber (Wang et al. 2006; Wang et al. 2004) and tleap (Case et al. 2008) modules were used to assign the generalized Amber force field (GAFF) (Wang et al. 2006; Wang et al. 2004) parameters (Appendixes 1 and 2) to the ligands, and ff03 parameters were assigned to 1A2. For the ligands, GAFF parameters were augmented with the partial atomic charges calculated at the ab-initio HF/6-31G\* theory level by use of Gaussian 03 (Frisch et al. 2004). The default protonation states were set at a neutral pH for all the ionizable residues. The heme cofactor is represented in all simulations with a modified Cys residue covalently bound to the heme iron, and its force field parameters were adopted from previously published work (Harris et al. 2004). The two systems were neutralized by adding six Cl<sup>−</sup> counter ions, and were surrounded by a periodic box of TIP3P water molecules extended 10 Å from the solute atoms.

All MD simulations were conducted by use of the standard procedure, which comprises energy-minimization, gradual heating of the complexes, and isothermal isobaric ensemble MD. First, the solvent molecules and counter ions were relaxed during a 2000-step minimization. The full systems were then minimized, to remove bad contacts in the initial geometry, by means of a conjugate gradient minimization of 2500 steps. Second, each system was

gradually heated from 0 to 300 K in 200 psec (ps) with solutes constrained at a weak constraint level of 5 kcal mol<sup>−1</sup> Å<sup>−2</sup>, followed by constant temperature equilibration at 300 K for 200 ps with solutes constrained at a weak constraint level of 2 kcal mol<sup>−1</sup> Å<sup>−2</sup>. Finally, periodic boundary dynamics simulations of 4 ns were carried out with an NPT (constant particle, pressure, and temperature) ensemble at 1 atm and 300 K. During the product simulation, temperature regulation was achieved by Langevin coupling with a collision frequency of 1.0 ps<sup>−1</sup> (Berendsen et al. 1984), and the SHAKE algorithm (Miyamoto and Kollman 1992) was used to constrain all bonds which contain hydrogen atoms. The particle–mesh–Ewald method (Darden et al. 1993) was used to treat long-range electrostatic interactions. A cut-off of 10 Å was used for the non-covalent interactions. Trajectories were sampled every 0.2 ps.

#### MM-PBSA/GBSA binding-free-energy calculations

In this study, the binding free energies ( $\Delta G_{\text{bind, pred}}$ ) of the receptor–ligand complexes were calculated by use of the MM-PBSA method (Fogolari et al. 2003; Liu et al. 2010; He et al. 2010; Neugebauer et al. 2008; Zeng et al. 2008; Rastelli et al. 2010). The MM-PBSA approach, which is encoded in the Amber 10.0 software, was used to compute the binding free energy between a ligand and its targeted protein, by using the 100 snapshots isolated from the final 1.0 ns period with an interval of 10 ps. All counterions and water molecules were stripped. A grid spacing of 0.5 Å was chosen, and the dielectric constants for the solute and solvent were set to 1 and 80, respectively. The optimized atomic radii set in Amber 10.0 were used. The electrostatic contribution to the solvation-free energy was determined by use of the PBSA module in the Amber 10.0 suite which numerically solves the Poisson–Boltzmann equations. For each snapshot, a free energy is calculated for each molecular species (complex, receptor, and ligand) and the ligand-binding free energy is calculated by use of the equation (Fogolari et al. 2003; Liu et al. 2010; He et al. 2010):

$$\Delta G_{\text{bind, pred}} = G_{\text{complex}} - [G_{\text{receptor}} + G_{\text{ligand}}] \quad (1)$$

The binding free energy contains an enthalpic and entropic contribution:

$$\Delta G_{\text{bind, pred}} = \Delta H - T\Delta S \quad (2)$$

The enthalpy of binding  $\Delta H$  is composed of  $\Delta G_{\text{MM}}$ , the change in the molecular mechanics free energy upon complex formation,  $\Delta G_{\text{solv}}$ , the solvated free energy contribution, and  $-T\Delta S$ , which represents the entropy term. The molecular mechanics free energy is calculated as follows:

$$\Delta G_{\text{MM}} = \Delta G_{\text{ele}} + \Delta G_{\text{vdw}} \quad (3)$$

where  $\Delta G_{\text{ele}}$  and  $\Delta G_{\text{vdw}}$  represent the Coulomb and van der Waals interactions, respectively. The solvation free energy is composed of two components:

$$\Delta G_{\text{sol}} = \Delta G_{\text{ele,sol}} + \Delta G_{\text{nonpol,sol}} \quad (4)$$

where  $\Delta G_{\text{ele,sol}}$  is the polar contribution to solvation and  $\Delta G_{\text{nonpol,sol}}$  is the nonpolar solvation term. The former could be obtained by solving the Poisson–Boltzmann equation for MM-PBSA method, whereas the latter term was determined by use of the equation:

$$\Delta G_{\text{nonpol,sol}} = \gamma \Delta \text{SASA} + b \quad (5)$$

where  $\gamma$ , which represents the surface tension, and  $b$ , a constant, were set to 0.0072 kcal/(mol Å<sup>2</sup>) and 0 (Still et al. 1990), respectively. SASA is the solvent-accessible surface area (Å<sup>2</sup>), and was estimated by use of the MSMS algorithm with a probe radius of 1.4 Å (Sanner et al. 1996).

In general, normal mode analysis is used to assess entropic changes of the solute molecule. However, this is computationally expensive and may generate a large margin of error that introduces significant uncertainty in the results (Neugebauer et al. 2008; Zeng et al. 2008; Rastelli et al. 2010). In this work, similar flavonoids binding to the same active site pocket of 1A2 resulted in similar entropy. The entropy involved in the calculation would not make much difference in comparison of the binding free energies of different ligands, so the entropy contribution was not considered in this work because of the similarity of the two systems studied.

The MM-GBSA (molecular mechanics and generalized Born surface area) procedure was performed to calculate the interaction energies in a free-energy-decomposition procedure between each ligand and each individual residue (Rastelli et al. 2010; Genheden and Ryde 2010; Fang et al. 2008). The binding interaction of each inhibitor–residue pair ( $G_{\text{inhibitor-residue}} = \Delta E_{\text{vdw}} + \Delta E_{\text{ele}} + \Delta G_{\text{GB}} + \Delta G_{\text{SA}}$ ) includes three terms: van der Waals contribution ( $\Delta E_{\text{vdw}}$ ), electrostatic contribution ( $\Delta E_{\text{ele}}$ ), and solvation contribution ( $\Delta G_{\text{GB}} + \Delta G_{\text{SA}}$ ), where  $\Delta E_{\text{vdw}}$  and  $\Delta E_{\text{ele}}$  are non-bonded van der Waals interactions and electrostatic

interactions between the inhibitor and each 1A2 residue, respectively, which can be computed by use of the sander module in Amber 10.0. The polar contribution ( $\Delta G_{\text{GB}}$ ) of desolvation was computed by using the generalized Born (GB) model, and the nonpolar contribution of desolvation ( $\Delta G_{\text{SA}}$ ) was computed by using the surface area. The charges used in GB calculations were taken from the Amber parameter set. All energy components were calculated using the same 100 snapshots as the MM-PBSA procedures. The free-energy-decomposition energy analysis can provide insight into the mechanisms of inhibition of 1A2 by oroxylin, wogonin, and/or ANF and elucidate the molecular basis for their different binding affinities by interpretation of structure and energy results.

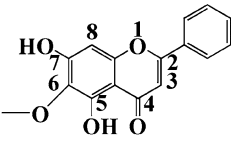
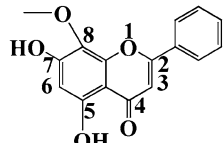
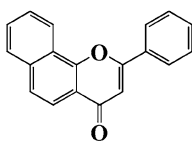
## Results

### Validation of molecular docking and molecular dynamics simulation methods

To validate whether the docking program MOE is sufficiently robust for the 1A2 system, the crystal pose of ANF was first re-docked into the binding-site pocket of 1A2 by use of a variety of docking conditions and scoring functions; these were then compared with the crystal pose. Docking is considered successful if the RMSD value of the optimum pose is smaller than a given threshold of 1.0 Å from the crystal pose after cluster analysis. The RMSD value of ANF between the optimum-docking pose and the crystal counterpart was 0.36 Å. This suggests that MOE reproduces the crystal-binding model well and is applicable to the 1A2 system. Subsequently, oroxylin and wogonin were docked into the same binding-site pocket of 1A2 with the same optimum docking parameters and scoring functions used above to generate the starting models for subsequent MD simulations (Fig. 1).

The dynamic stability of the 1A2–oroxylin and 1A2–wogonin complexes was monitored by examination of the time-dependent RMSD profiles from the X-ray crystal structure of 1A2 during MD trajectories of 4.0 ns. As

**Fig. 1** The chemical structures, binding free energies, and experimental inhibitory affinities (IC<sub>50</sub>) (Li et al. 2008) of oroxylin, wogonin, and  $\alpha$ -naphthoflavone toward human cytochrome P450 1A2

			
	oroxylin	wogonin	$\alpha$ -naphthoflavone
<b>Predicted binding free energy (kcal/mol)</b>	<b>-19.8</b>	<b>-21.1</b>	<b>-23.5</b>
<b>Experimental IC<sub>50</sub> (nM)</b>	<b>579</b>	<b>248</b>	<b>49</b>





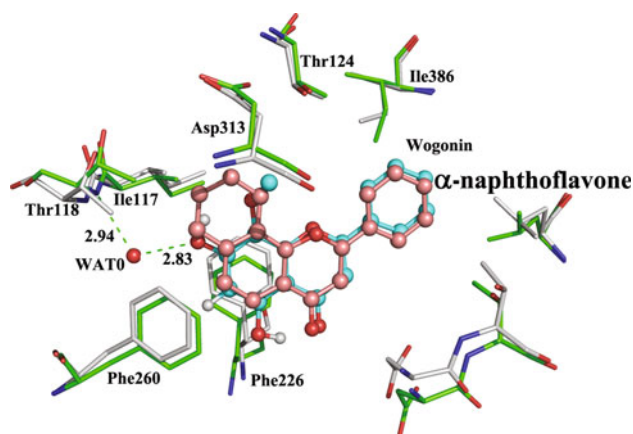


**Fig. 4** The binding mode of wogonin (CPK, carbon: cyan, oxygen: red, and hydrogen: gray) within the active site pocket of human cytochrome P450 1A2 after superposition of the crystal structure (gray) of 1A2 over the MD simulated model (green) in the complex with wogonin.  $\alpha$ -Naphthoflavone (CPK, carbon: magenta and oxygen: red) is displayed within the active site pocket of 1A2. For clarity, residues Gly316 and Ala317 over the two ligands have been omitted

Ile117, Thr118, Ser122, Thr124, Phe125, Phe226, Phe256, Phe260, Leu261, Asn312, Asp313, Gly316, Ala317, Phe319, Thr321, Leu382, Ile386, Leu497, and the heme, accommodates the polycyclic aromatic ring of wogonin. As shown in Fig. 4, both orthogonal and parallel aromatic interactions between wogonin and the phenyl side chains of Phe125 and Phe226 are observed in the simulated model. The van der Waals and hydrophobic interactions with the Gly316–Ala317 peptide bond, hold the aromatic ring of wogonin within the active site pocket (Fig. 3a and 4). A water molecule WAT0 forms three hydrogen bonds ( $H1 = 2.83$  Å,  $H2 = 2.75$  Å, and  $H3 = 2.94$  Å) with the phenolic hydroxyl O7 atom of oroxylin, the OD1 atom of Asn257, and the N atom of Thr118, respectively.

#### *Oroxylin binds differently from ANF*

In the crystal structure of 1A2 with bound ANF, Thr118, Ser122, and Thr124 are the main candidates to form polar contacts with ligands. Among these, Thr118 is one of the closest residues to ANF. In the initial docking model of the 1A2–oroxylin complex, the distance of 3.3 Å between the CG2 atom of Thr118 and the methoxy group at the 6 position of the oroxylin ring may cause energetically unfavorable repulsion. To reduce unfavorable repulsion, oroxylin rotated in a clockwise direction (Fig. 5a) to interact directly with Asp313 and significant conformational changes in the side-chain of Thr118 were observed (Fig. 5b) compared with that in the crystal structure of 1A2; this may have slightly reduced the inhibitory affinity of oroxylin.

The OD1 atom of Asp313 forms a strong hydrogen bond ( $H4$ ) 2.66 Å long with the O7 atom of oroxylin, and its

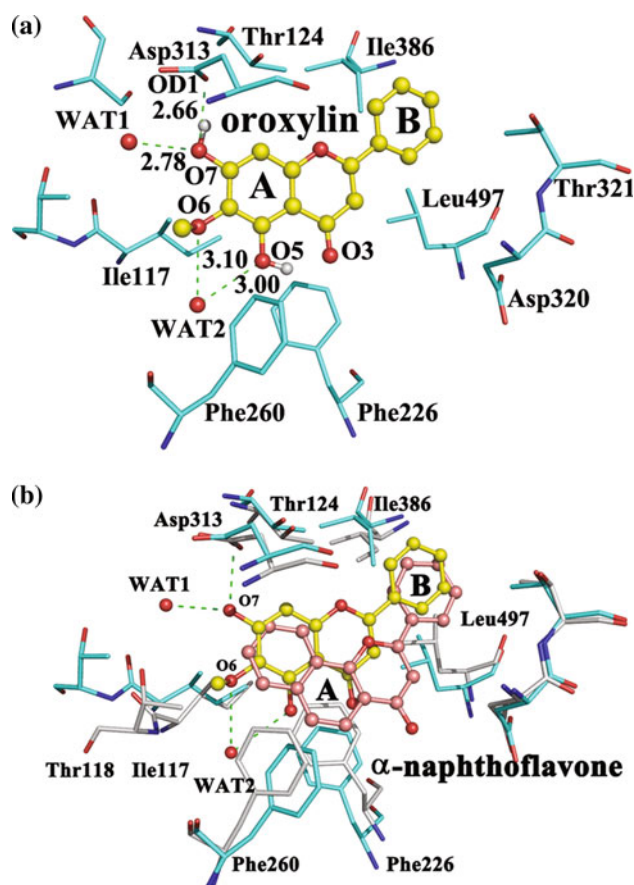


**Fig. 5** (a) The binding mode of oroxylin (CPK, carbon: yellow, oxygen: red, and hydrogen: gray) within the active site pocket of human cytochrome P450 1A2 after superposition of the X-ray crystal structure of 1A2 (gray) over the MD simulated model (green) in complex with oroxylin. In (b),  $\alpha$ -naphthoflavone (CPK, carbon: pink and oxygen: red) is displayed within the active site pocket of 1A2. For clarity, residues Gly316 and Ala317 over the two ligands have been omitted

adjacent OD2 atom is also located within a hydrogen-bonding distance ( $H5$ ) of 3.47 Å from oroxylin's O7 atom. As shown in Fig. 3b, a water molecule WAT1 forms two hydrogen bonds ( $H6 = 2.78$  Å and  $H7 = 2.84$  Å, respectively) with the O7 atom of oroxylin and the OD2 atom of Asp313. Additionally, both the O5 and O6 atoms of oroxylin are involved in hydrogen-bonding interactions with another water molecule WAT2 ( $H8 = 3.00$  Å and  $H9 = 3.10$  Å, respectively). The aforementioned hydrogen-bonding interactions are not observed in the crystal structure of 1A2 with bound ANF. With the exception of the hydrogen-bonding interactions, most of the van der Waals and hydrophobic interactions between residues Phe226, Ala317, Gly316, Leu497, Phe125, and Phe260 and ANF are conserved in the 1A2–oroxylin and 1A2–ANF complexes (Fig. 3b and 5b). As a result, van der Waals, hydrophobic, and hydrogen-bonding interactions may explain the mechanism of inhibition of oroxylin.

## Binding-free-energy analysis using the MM-PBSA method

To obtain further information about the contributions of each component to the 1A2–oroxylin and 1A2–wogonin complexes, binding-free-energy calculations using the MM-PBSA method were performed. Table 1 lists the binding free energies predicted by MM-PBSA ( $\Delta G_{\text{bind, pred}}$ ) and the decomposition of energy terms, which were averaged over 100 snapshots for the final 1.0 ns (every 10 ps) MD simulations. It is clear that the  $\Delta E_{\text{ele}}$ ,  $\Delta E_{\text{vdw}}$ , and  $\Delta G_{\text{ele, sol}}$  components make the major contributions to the total binding free energy. The electrostatic interaction energy ( $\Delta E_{\text{ele}}$ ) for the 1A2–oroxylin complex is 6.4 kcal/mol smaller than that for the 1A2–wogonin complex, and the difference of 6.3 kcal/mol between the van der Waals interactions ( $\Delta E_{\text{vdw}}$ ) for the two complexes may counteract the trend in the electrostatic interactions.

The experimental  $\text{IC}_{50}$  values for oroxylin and wogonin against 1A2 are 579 and 248 nM (Fig. 1) (Li et al. 2008), respectively. The latter was twice as potent as the former. A less negative value (−19.8 kcal/mol) of  $\Delta G_{\text{bind, pred}}$  for the 1A2–oroxylin complex was obtained than that (−21.1 kcal/mol) for the 1A2–wogonin complex. Consequently, the energy results imply the 1A2 prefers wogonin to oroxylin, which is compatible with our previous experimental assays. Our results indicate that MD simulations and binding-free-energy calculations can provide an alternative approach to assessing the inhibitory affinities of flavonoids towards 1A2.

## Residue-based-energy decomposition using the MM-GBSA method

To further evaluate the effects of energy on the contributions of each residue in the binding-site pocket, residue-

**Table 1** Components of the binding free energy (kcal/mol) for human cytochrome P450 1A2 in complexes with oroxylin or wogonin, determined by use of the MM-PBSA method

Ligand	Oroxylin	Wogonin	$\alpha$ -Naphthoflavone
$\Delta E_{\text{ele}}$	$-12.2 \pm 2.9$	$-5.9 \pm 1.9$	$-0.7 \pm 1.7$
$\Delta E_{\text{vdw}}$	$-41.6 \pm 2.5$	$-47.9 \pm 1.8$	$-47.6 \pm 1.6$
$\Delta G_{\text{nonpol, sol}}$	$-5.3 \pm 0.1$	$-4.9 \pm 0.1$	$-5.1 \pm 0.1$
$\Delta G_{\text{ele, sol}}$	$39.3 \pm 2.7$	$37.3 \pm 2.7$	$28.9 \pm 2.6$
$\Delta G_{\text{bind, pred}}$	$-19.8 \pm 3.7$	$-21.1 \pm 3.1$	$-23.5 \pm 3.0$
$\Delta G_{\text{bind, exp}}$	−8.8	−9.3	−10.4

MM-PBSA, molecular mechanical and Poisson Boltzmann/surface accessible

$\Delta E_{\text{ele}}$ , electrostatic interactions calculated by use of the MM force field;  $\Delta G_{\text{vdw}}$ , van der Waals' contributions from MM;  $\Delta G_{\text{nonpol, sol}}$ , the nonpolar contribution to solvation;  $\Delta G_{\text{ele, sol}}$ , the polar contribution to solvation;  $\Delta G_{\text{bind, pred}}$ , the predicted binding free energies with the entropic contribution omitted;  $\Delta G_{\text{bind, exp}}$  was estimated approximately via  $\Delta G_{\text{bind, exp}} \approx RT \ln \text{IC}_{50}$

based energy decomposition for the binding free energies between the ligands and 1A2 was conducted by use of the MM-GBSA method. Figure 6 shows the energy decomposition for key residues in the two complexes.

In general, if the interaction energy between a residue and a ligand is lower than −1 kcal/mol, the residue is considered to be important in the molecular recognition of ligands. For the 1A2–oroxylin complex, major favorable energy contributions (−3.0 to −0.8 kcal/mol) originate predominately from Asp313 (−2.8), Ala317 (−1.8), Phe226 (−1.3), Ile117 (−1.2), Gly316 (−1.2), Phe125 (−1.1), heme (−1.0), and Leu497 (−1.0). In the binding model of oroxylin, Asp313 forms two hydrogen bonds with oroxylin, which results in a favorable energy contribution of −2.8 kcal/mol to the total binding free energy. Additionally, oroxylin involves hydrophobic interactions with the adjacent residues Ala317, Phe226, Ile117, Gly316, Phe125, and heme, which achieves more than 1 kcal/mol enhancement of the energy favorable to the absolute total binding free energy. From these results, one can conclude that the van der Waals and hydrophobic interactions may be more important than the hydrogen-bonding interactions in the mechanism of inhibition of 1A2 by oroxylin.

In the 1A2–wogonin complex, as expected, except for Asp313 and Phe226 most of the residues make energy contributions similar to those in the 1A2–oroxylin complex. In the 1A2–wogonin complex, Asp313 does not form a hydrogen bond with wogonin, so there is an absolute difference of 2.6 kcal/mol in the binding free energy between Asp313 and oroxylin/wogonin. Additionally, a strong  $\pi$ – $\pi$  stacking interaction between Phe226 and the aromatic ring of wogonin results in a relative negative binding free energy of −3.2 kcal/mol. The eight residues Phe226 (−3.2), Ala317 (−1.7), Gly316 (−1.5), Leu497 (−1.3), Phe125 (−1.1), Phe260 (−1.1), Thr124 (−1.0), and Ile117 (−1.0) give the most negative binding free energies (Fig. 6), and all of these involve van der Waals contacts with wogonin. This can aid understanding of why the  $\Delta E_{\text{vdw}}$  term for wogonin in Table 1 is −47.9 kcal/mol, and why the van der Waals and hydrophobic forces are the primary factors explaining the mechanism of inhibition by wogonin.

## Discussion

The larger binding-site pocket of the 1A2–oroxylin complex could account for why oroxylin has weaker inhibitory activity than wogonin and ANF

In 1A2–oroxylin, the sidechain of Thr118 undergoes significant conformational changes to reduce energetically unfavorable repulsion with the methoxy group at the 6

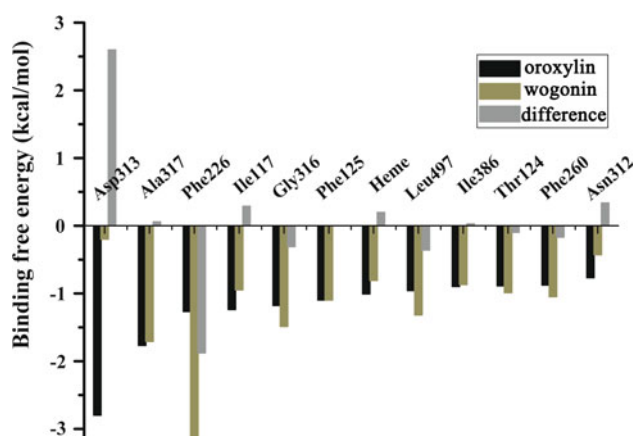


**Fig. 6** Residue-based energy decomposition for key residues for the human cytochrome P450 1A2–oroxylin and 1A2–wogonin complexes

position of the oroxylin ring. Thus it is reasonable to speculate that oroxylin may result in a larger binding-site pocket than ANF. By using the promomol approach (Liu et al. 2010; He et al. 2010; Jain 2007) embedded in Tripos Sybyl 7.3.5, the volume of the crystal binding-site pocket of 1A2 was estimated to be 415.8 Å<sup>3</sup> after ANF was omitted, whereas those of the simulated 1A2–wogonin and 1A2–oroxylin complexes were 477.7 and 587.3 Å<sup>3</sup> under identical conditions. The order in the volumes of the binding-site pockets of the three complexes is compatible with the experimental inhibitory trend (49 nM < 248 nM < 579 nM) (Li et al. 2008). Accordingly, the larger and much more open binding-site architecture of the 1A2/oroxylin complex weakens the van der Waals and hydrophobic interactions between 1A2 and oroxylin, in contrast with the rather compact and closed binding-site topology of 1A2.

ANF binds more strongly to 1A2 than wogonin and oroxylin

The experimental IC<sub>50</sub> value of ANF against 1A2 is 49 nM (Fig. 1) (Li et al. 2008; Liu et al. 2010; He et al. 2010). It is five times more potent than wogonin. To obtain a direct reference, the 1A2–ANF complex was subjected to the MD and MM-PBSA/GBSA procedures under identical conditions. Similarly, the antechamber and tleap modules were used to assign the GAFF parameters (Appendix 3) to ANF. Notably, the MD model seemed to reach a stable state after 1 ns equilibration, in which the RMSD values converged below 1.5 Å (Appendix 4) and the MD simulated model can support the crystal structure of 1A2.

No hydrogen bond is observed between ANF and its adjacent residues, and the van der Waals and hydrophobic interactions are dominant in the mechanism of inhibition by ANF. Its predicted binding free energy is −23.5 kcal/

mol and more negative than that (−21.1 kcal/mol) of wogonin, which corresponds to enhancement of inhibitory affinity. Because of the smaller  $\pi$ – $\pi$  flavone system of wogonin, binding-free-energy values of some of the residues are less negative than those in the 1A2–ANF complex. As a result, reduction of van der Waals and hydrophobic interactions can explain why wogonin binds less strongly to the enzyme 1A2 and why wogonin has a weaker inhibitory affinity than ANF.

$\Delta G_{\text{bind, exp}}$  in Table 1 was estimated approximately by use of  $\Delta G \approx RT \ln \text{IC}_{50}$  for direct comparison. The  $\Delta G_{\text{bind, exp}}$  values are −8.8, −9.3, and −10.4 kcal/mol for CYP 1A2 in complexes with oroxylin, wogonin, and ANF, respectively, and the relevant  $\Delta G_{\text{bind, pred}}$  values are −19.8, −21.1, and −23.5 kcal/mol, respectively. The descending trend in  $\Delta G_{\text{bind, exp}}$  for those complexes was consistent with that in  $\Delta G_{\text{bind, exp}}$ . In this work, the entropic contribution ( $T\Delta S$ ) was omitted, and the  $\Delta G_{\text{bind, pred}}$  values were more negative than those estimated on the basis of the experimental IC<sub>50</sub> values. However, it is still of significance to compare their relative magnitudes, which is common in the literature (Fogolari et al. 2003; Liu et al. 2010; He et al. 2010; Neugebauer et al. 2008; Zeng et al. 2008; Rastelli et al. 2010).

By default, the final energy after docking was evaluated using the generalized Born solvation (GB/VI) model in MOE (MOE 2008; Labute 2008). The GB/VI binding free energies were −23.63, −27.42, and −27.15 kcal/mol for CYP 1A2 in complexes with oroxylin, wogonin, and ANF, respectively. As a result, their order is not consistent with those of  $\Delta G_{\text{bind, pred}}$  predicted from the MM-PBSA approach and  $\Delta G_{\text{bind, exp}}$  estimated from experimental binding affinities; this suggests that GB/VI binding free energy calculations may be not suitable for the three ligands in the CYP 1A2 system.

## Conclusion

Structural analysis reveals that wogonin binds to 1A2 in a similar manner to ANF, whereas the pattern is slightly different for oroxylin. Compared with ANF, oroxylin is rotated when forming hydrogen bonds with Asp313 and a water molecule at the O5 and O6 positions, which is not observed in the 1A2–ANF and 1A2–wogonin complexes. The more open binding-site pocket of the 1A2–oroxylin complex, in contrast with the rather closed binding-site topology of apo-1A2, could account for why oroxylin has weaker inhibitory activity against 1A2 than ANF and wogonin.

The MM-PBSA calculations predicted binding free energies of −23.5 (ANF), −21.1 (wogonin), and −19.8 (oroxylin) kcal/mol which are consistent with our previous



experimental assays (49 nM, 248 nM, and 579 nM) (Li et al. 2008). Our energy analysis also revealed that several residues (Asp313, Ala317, Phe226, Ile117, Gly316, and Phe125) and the heme are important in the mechanism of inhibition by oroxylin via hydrogen-bonding, van der Waals, and hydrophobic interactions.

**Acknowledgments** We are grateful for financial support from the Natural Science Foundation of China (21103234), the Natural Science Foundation of Guangdong Province (S2011030003190), the Science Foundation of the Department of Education in Guangdong Province (CXZD1006), the Science Foundation of Guangzhou City (2010Y1-C531), and Fundamental Research Funds for the Central Universities (10ykjc20).

## References

- Arimoto R (2006) Computational models for predicting interaction with cytochrome P450 enzyme. *Curr Top Med Chem* 6:1909–1918
- Babu TH, Rao VRS, Tiwari AK, Babu KS, Srinivas PV, Ali AZ, Rao JM (2008) Synthesis and biological evaluation of novel 8-aminomethylated oroxylin A analogues as alpha-glucosidase inhibitors. *Bioorg Med Chem Lett* 18:1659–1662
- Berendsen HJC, Postma JPM, van Gunsteren WF, DiNola A, Haak JR (1984) Molecular dynamics with coupling to an external bath. *J Chem Phys* 81:3684–3690
- Birt DF, Hendrich S, Wang W (2001) Dietary agents in cancer prevention: flavonoids and isoflavonoids. *Pharmacol Ther* 90:157–177
- Butler MA, Iwasaki M, Guengerich FP, Kadlubar FF (1989) Human cytochrome P-450PA (P-450IA2), the phenacetin O-deethylase, is primarily responsible for the hepatic 3-demethylation of caffeine and N-oxidation of carcinogenic arylamines. *Proc Natl Acad Sci USA* 86:7696–7700
- Case DA, Darden TA, Cheatham TE III et al (2008) AMBER 10. University of California, San Francisco
- Cho US, Park EY, Dong MS, Park BS, Kim K, Kim KH (2003) Tight-binding inhibition by alpha-naphthoflavone of human cytochrome P450 1A2. *Biochim Biophys Acta* 1648:195–202
- Darden T, York D, Pedersen L (1993) Particle mesh Ewald: an  $N \log(N)$  method for Ewald sums in large systems. *J Chem Phys* 98:10089–10092
- Eaton DL, Gallagher EP, Bammler TK, Kunze KL (1995) Role of cytochrome P450 1A2 in chemical carcinogenesis: implications for human variability in expression and enzyme activity. *Pharmacogenet Genom* 5:259–274
- Faber MS, Jetter A, Fuhr U (2005) Assessment of 1A2 activity in clinical practice: why, how, and when? *Basic Clin Pharmacol Toxicol* 97:125–134
- Fang L, Zhang H, Cui W, Ji MJ (2008) Studies of the mechanism of selectivity of protein tyrosine phosphatase 1B (PTP1B) bidentate inhibitors using molecular dynamics simulations and free energy calculations. *J Chem Info Model* 48:2030–2041
- Fogolari F, Brigo A, Molinari H (2003) Protocol for MM/PBSA molecular dynamics simulations of proteins. *Biophys J* 85:159–166
- Frisch MJ, Trucks GW, Schlegel HB et al (2004) Gaussian 03, Revision E01. Gaussian, Inc, Pittsburgh PA
- Genheden S, Ryde U (2010) How to obtain statistically converged MM/GBSA results. *J Comput Chem* 31:837–846
- Harris DL, Park JY, Gruenke L, Waskell L (2004) Theoretical study of the ligand-CYP2B4 complexes: effect of structure on binding free energies and heme spin state. *Proteins* 55:895–914
- He F, Bi HC, Xie ZY, Zuo Z, Li JK, Li X, Zhao LZ, Chen X, Huang M (2007) Rapid determination of six metabolites from multiple cytochrome P450 probe substrates in human liver microsome by liquid chromatography/mass spectrometry: application to high-throughput inhibition screening of terpenoids. *Rapid Commun Mass Spectrom* 21:635–643
- He L, He F, Bi H, Li J, Zeng S, Luo HB, Huang M (2010) Isoform-selective inhibition of chrysin towards human cytochrome P450 1A2. Kinetics analysis, molecular docking, and molecular dynamics simulations. *Bioorg Med Chem Lett* 20:6008–6012
- Heim KE, Tagliaferro AR, Bobilya DJ (2002) Flavonoid antioxidants: chemistry, metabolism and structure-activity relationships. *J Nutr Biochem* 13:572–584
- Hong CC, Tang BK, Hammond GL, Trichtler D, Yaffe M, Boyd NF (2004) Cytochrome P450 1A2 (CYP1A2) activity and risk factors for breast cancer: a cross-sectional study. *Breast Cancer Res* 6:R352–R365
- Ioria F, da Fonseca R, Joao Ramos M, Menziani MC (2005) Theoretical quantitative structure–activity relationships of flavone ligands interacting with cytochrome P450 1A1 and 1A2 isozymes. *Bioorg Med Chem* 13:4366–4374
- Jain AN (2007) Surflex-Dock 2.1: robust performance from ligand energetic modeling, ring flexibility, and knowledge-base search. *J Comput Aid Mol Des* 21:281–306
- Kemp CA, Flanagan JU, van Eldik AJ, Maréchal JD, Wolf CR, Roberts GCK, Paine MJI, Sutcliffe MJ (2004) Validation of model of cytochrome P450 2D6: an in silico tool for predicting metabolism and inhibition. *J Med Chem* 47:5340–5346
- Kunze LK, William FT (1993) Isoform-selective mechanism-based inhibition of human cytochrome P450 1A2 by furafylline. *Chem Res Toxicol* 6:649–656
- Labute P (2008) The generalized Born/volume integral implicit solvent model: estimation of the free energy of hydration using London dispersion instead of atomic surface area. *J Comput Chem* 29(10):1693–1698
- Li HB, Chen F (2005) Isolation and purification of baicalein, wogonin and oroxylin A from the medicinal plant *Scutellaria baicalensis* by high-speed counter-current chromatography. *J Chromatogr A* 1074:107–110
- Li JK, He F, Bi HC, Zuo Z, Liu BD, Luo HB, Huang M (2008) Inhibition of human cytochrome P450 CYP 1A2 by flavonoids: a quantitative structure-activity relationship study. *Acta Pharm Sin* 43:1198–1204
- Lin CC, Shieh DE (1996) The anti-inflammatory activity of *Scutellaria rivularis* extracts and its active components, baicalin, baicalein, and wogonin. *Am J Chin Med* 24:31–36
- Liu M, Yuan M, Luo M, Bu X, Luo HB, Hu X (2010) Binding of curcumin with glyoxalase I: molecular docking, molecular dynamics simulations, and kinetics analysis. *Biophys Chem* 147:28–34
- Li-Weber M (2009) New therapeutic aspects of flavones: the anticancer properties of *Scutellaria* and its main active constituents wogonin, baicalein and baicalin. *Cancer Treat Rev* 35:57–68
- Miyamoto S, Kollman PA (1992) Settle: an analytical version of the SHAKE and RATTLE algorithm for rigid water models. *J Comput Chem* 13:8952–8962
- MOE 2008.10 (2008) Chemical Computing Group Inc., Montreal, Quebec, Canada
- Moon YJ, Wang X, Morris ME (2006) Dietary flavonoids: effects on xenobiotic and carcinogen metabolism. *Toxicol In Vitro* 20:187–210

- Neugebauer RC, Uchieczowska U, Meier R et al (2008) Structure-activity studies on splitomicin derivatives as sirtuin inhibitors and computational prediction of binding mode. *J Med Chem* 51:1203–1213
- Park H, Lee S, Suh J (2005) Structural and dynamical basis of broad substrate specificity, catalytic mechanism, and inhibition of cytochrome P450 3A4. *J Am Chem Soc* 127:13634–13642
- Rastelli G, Del RA, Degliesposti G, Sgobba M (2010) Fast and accurate predictions of binding free energies using MM-PBSA and MM-GBSA. *J Comput Chem* 31:797–810
- Sanner MF, Olson AJ, Spehner JC (1996) Reduced surface: an efficient way to compute molecular surfaces. *Biopolymers* 38:305–320
- Sansen S, Yano JK, Reynald RL, Schoch GA, Griffin KJ, Stout CD, Johnson EF (2007) Adaptations for the oxidation of polycyclic aromatic hydrocarbons exhibited by the structure of human P450 1A2. *J Biol Chem* 282:14348–14355
- Si DY, Wang Y, Zhou YH, Guo Y, Wang J, Zhou H, Li ZS, Fawcett JP (2009) Mechanism of CYP2C9 inhibition by flavones and flavonols. *Drug Metab Disp* 37:629–634
- Still WC, Tempczyk A, Hawley RC, Hendrickson T (1990) Semi-analytical treatment of solvation for molecular mechanics and dynamics. *J Am Chem Soc* 112:6127–6129
- Wang J, Wolf RM, Caldwell JW, Kollman PA, Case DA (2004) Development and testing of a general AMBER force field. *J Comput Chem* 25:1157–1174
- Wang J, Wang W, Kollman PA, Case DA (2006) Automatic atom type and bond type perception in molecular mechanical calculations. *J Mol Graph Model* 25:247–260
- Wolf CR, Smith G, Smith RL (2000) Science, medicine and the future pharmacogenetics. *Br Med J* 320:987–990
- Zeng J, Li W, Zhao Y, Liu G, Tang Y, Jiang H (2008) Insights into ligand selectivity in estrogen receptor isoforms: molecular dynamics simulations and binding free energy calculations. *J Phys Chem B* 112:2719–2726